Proceedings of the ASME 2023 42nd International Conference on Ocean, Offshore and Arctic Engineering
OMAE2023
June 11-16, 2023, Melbourne, Australia

OMAE2023-108097

A SYSTEMATIC APPROACH FOR DEVELOPING A NUMERICAL WAVETANK TO SIMULATE DRIVEN SHALLOW- AND DEEP-WATER WAVES

Wajiha Rehman[1]*†, Onno Bokhove[1]*†, Mark Kelmanson[1]†

[1]Leeds Institute for Fluid Dynamics, Leeds, UK

ABSTRACT

Numerical models of wavetanks for nonlinear waves driven by waveflap/piston wavemakers are developed. Variational principles (VPs) for the underlying equations of nonlinear potential-flow dynamics are implemented directly in the finite-element-based environment Firedrake*. The establishment of mathematical and numerical wavetank models, based on VPs and domain-specific compiler architecture, is a novel challenge aimed at both reducing time-to-development and enabling new model experimentation. The waveflap-wavemaker problem is fundamentally more complex than the piston-wavemaker problem since reformulation of the mathematical problem into a computational domain respectively demands multi- and single-step transformations because of the respective two- and one-dimensional wavemaker motions. Hence this paper presents a systematic approach for developing a numerical piston/waveflap wavemaker wavetank, within the widely available* Firedrake *environment, that can simulate the dynamics of both shallow- and deep-water waves. Updated pre-print with extra appendices of* https://doi.org/10.1115/OMAE2023-108097

Keywords: Numerical wavetank, numerical fluid dynamics, shallow-water equations, potential-flow theory.

1. INTRODUCTION

The maritime industry frequently uses laboratory wavetanks to study water waves and their interactions with maritime structures in a controlled experimental environment. Performing such laboratory experiments is expensive and time-consuming, potentially impeding the acquisition of sufficient experimental data. Hence, mathematical and numerical models of wavetanks are extensively used to facilitate initial design processes, and to validate and augment laboratory wavetank experiments.

A typical wavetank is a water-filled tank, one or two sides of which comprise a wavemaker that generates controllable waves; the other sides have wave-absorbing features such as solid boundaries or porous beaches. Wavetanks of different shapes and dimensions are equipped with different types of wavemakers to simulate specific sea states, as specified by the relation between water depth, amplitude and wavelength of the modelled water waves. To model shallow-water waves, wavetanks are equipped with piston-type wavemakers; and, to model intermediate-depth or deep-water waves, wavetanks tend to be equipped with waveflap-type wavemakers. Fig. 1 shows a wavetank, with wavemakers, at the Maritime Research Institute Netherlands (MARIN); data-generating experiments in a MARIN tank are the subject of a companion paper [1].

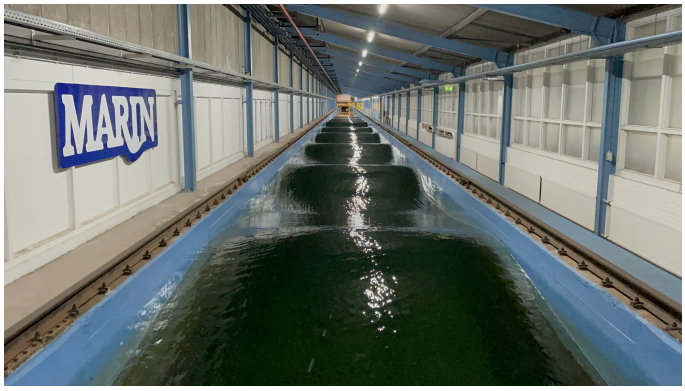

FIGURE 1: WATER WAVES GENERATED IN A RECTANGULAR WAVETANK AT MARIN. PHOTO COURTESY OF MARIN.

The dynamics of nonlinear water waves are governed by a variational principle (VP) or approximations thereof. Principally, we use the VP of Luke [2], extended to include piston and waveflap wavemakers as moving-boundary conditions. The use of a VP places emphasis on the conservative structure of nonlinear water-wave dynamics, since energy and mass conservation, as well as the conservation of phase-space volume, are intimately connected with this structure. The preservation of these conservation properties in the numerical discretisation ensures that

†Joint first authors
*Corresponding author: o.bokhove@leeds.ac.uk

simulations are compatible with the continuum dynamics, facilitating accuracy and stability. Several groups have therefore based their numerical discretisations directly on space and/or space-time discrete analogues of the underlying VP or associated Hamiltonian dynamics, see, e.g. [3, 4] and references therein for potential-flow dynamics in a vertical cross-section and for Hamiltonian Boussinesq dynamics in [5]. Such an approach based on VPs that generate the dynamics can be extended to include water-wave interactions with floating and flexible structures such as ships and offshore wind-turbine masts. However, the time-to-development of stand-alone special-purpose numerical implementations of numerical techniques, including those based on variational techniques for such maritime applications, can be substantial. A solution to the variational issue is to use a domain-specific compiler architecture, e.g. for the implementation of finite-element methods, because both finite-element methods and VPs are naturally aligned integral methods. *Firedrake* is one such "*automated system for the solution of partial differential equations using the finite element method (FEM).* Firedrake *uses sophisticated code generation*"[1].

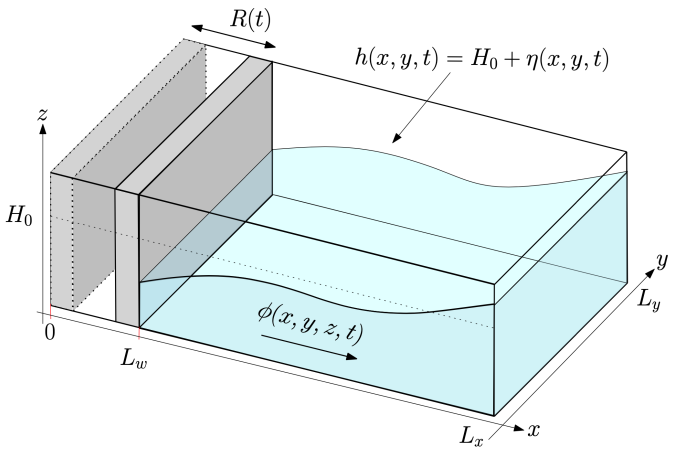

FIGURE 2: SCHEMATIC OF A RECTANGULAR WAVETANK WITH PISTON WAVEMAKER AT $x = R(t)$. THE PISTON WAVEMAKER OSCILLATES HORIZONTALLY IN $0 \leq x \leq L_w < L_x$ TO GENERATE WATER WAVES. THE VERTICAL COORDINATE IS z. THE FREE SURFACE RESIDES AT $z = h(x,y,t)$ ABOVE A FLAT BOTTOM AT $z = 0$; t IS TIME, y THE LATERAL HORIZONTAL COORDINATE AND THE VELOCITY POTENTIAL IS $\phi(x,y,z,t)$. THE DEPTH AT REST IS H_0, WHICH DEFINES A PERTURBATION η OF THE FREE SURFACE FROM REST. THE LATERAL EXTENT OF THE TANK IS L_y.

Hitherto, we have used *Firedrake* [6] to numerically implement three-dimensional potential-flow water-wave dynamics by deriving weak formulations systematically from Luke's VP and using *Firedrake* to facilitate efficient code generation. Subsequently, we have successfully validated numerical simulations against rogue waves generated by a piston wavemaker in MARIN's experimental wavetank. Luke's VP in the three-dimensional domain, with its moving free surface and piston wavemaker boundary, is first transformed into a VP with a fixed computational domain, a transformation also used in [7] to transform the original equations of motion. The spatial numerical discretisation consists of the use of higher-order Lagrange polynomials over one element in the vertical while using first-order continuous Galerkin Lagrange polynomials over a large number of finite elements in the horizontal. The algebra involved in deriving these weak formulations from the transformed VP is cumbersome and extensive. The aforementioned transformation – from the moving domain with a piston wavemaker and free surface into the fixed computational domain – is illustrated in Figs. 2 and 3. It is also used to transform the VP. Similarly, the moving domain with a waveflap wavemaker and free surface shown in Fig. 4 can be transformed into the fixed computational domain of Fig. 3 but the corresponding transformation of the VP is considerably more complex as a consequence of the two-dimensionality of the waveflap motion.

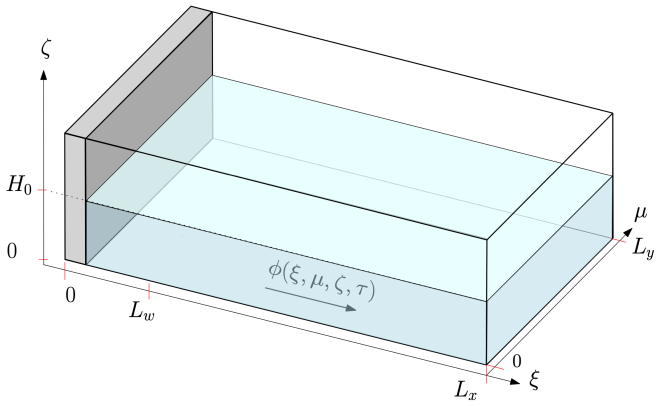

FIGURE 3: SCHEMATIC OF THE STATIC COMPUTATIONAL DOMAIN CORRESPONDING TO A RECTANGULAR WAVETANK WITH PISTON WAVEMAKER. TRANSFORMED SPATIAL COORDINATES ARE ξ, μ, ζ.

Our goals are therefore twofold: to outline the VP for water-wave dynamics including, as a novel aspect, a waveflap wavemaker (representing nonlinear reality as opposed to a linearised boundary condition); and, subsequently, to describe a systematic and novel numerical approach based on implementing space-time discrete VPs directly into *Firedrake* rather than weak formulations. Instead, the relevant weak forms are subsequently, and after specification of the (time-)discrete VP, derived automatically within the *Firedrake* architecture, rather than derived and implemented explicitly by the user, thereby reducing both the likelihood of human error and the time taken to develop and to implement code. In addition, this novel approach holds promise for future extensions, within manageable development times, to numerical monolithic models of fluid-structure-interactions based on coupled VPs for fluid and structure.

The outline of the paper is as follows. In §2, we review the variational principles (VPs) for potential-flow dynamics generated by wavemakers, as well as relevant transformed versions, and VPs, for simplified shallow-water dynamics. In §3, the numerical modelling is explained, starting with simplified shallow-water and ending with potential-flow dynamics. Preliminary numerical

[1] http://firedrakeproject.org/index.html

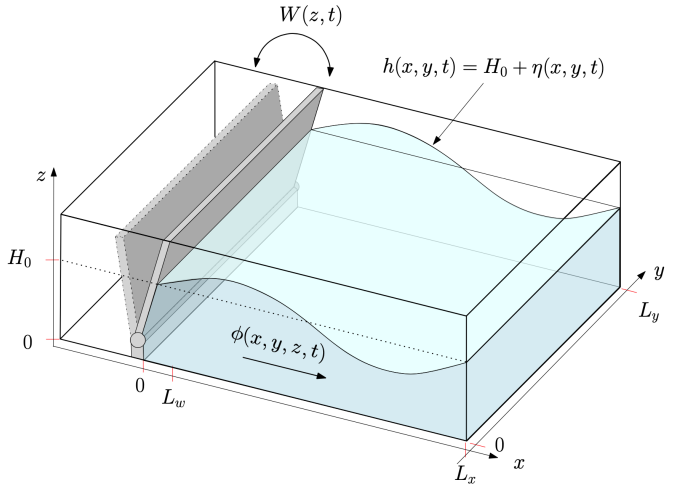

FIGURE 4: SCHEMATIC WAVETANK WITH WAVEFLAP WAVEMAKER, AT ITS LEFT-HAND END, HAVING POSITION $x = W(z,t)$; IT IS THIS RELATIONSHIP THAT BINDS TWO SPATIAL COORDINATES.

tests are shown in §4 before conclusions are drawn in §5.

2. VARIATIONAL MODELLING OF WATER WAVES

2.1 Potential-flow dynamics

Luke's variational principle [2] initiates the development of a numerical wavetank for inviscid, potential-flow fluid dynamics in a three-dimensional domain; its dynamics are given by the variation of the space-time integral expression, or VP,

$$\begin{aligned} 0 =& \delta \int_0^T \mathscr{L}\,[\phi, h]\,\mathrm{d}t = \delta \int_0^T \iiint_\Omega \partial_t \phi + \frac{1}{2}|\boldsymbol{\nabla}\phi|^2 \\ &+ g(z - H_0)\,\mathrm{d}z\,\mathrm{d}x\,\mathrm{d}y\,\mathrm{d}t, \end{aligned} \tag{1}$$

where $\mathscr{L} = \mathscr{L}[\phi, h]$ is the functional depending on variables h and ϕ in the spatial domain Ω. The transformation of the functional $\mathscr{L}$ of the VP (1) to a fixed domain can lead to differing levels of complexity depending on the case considered, as follows.

When the free surface is assumed single-valued, given by $z = h(x,y,t)$, and waves are driven by a piston wavemaker at $x = R(t)$, coordinates x and z are transformed as follows (cf. [8])

$$\hat{x} = \big(x - \tilde{R}(t)\big)\, L_w/(L_w - \tilde{R}(t)), \quad \hat{y} = y, \tag{2a}$$

$$\hat{z} = zH_0/h(x,y,t), \quad \hat{t} = t, \tag{2b}$$

with $\tilde{R}(t) = R(t)$ for $x \le L_w \le L_x$ and $\tilde{R}(t) = 0$ for $x > L_w$; this limits the transformed region affected by the wavemaker motion. The transformed VP is derived and given in [6, 8]. Considering a y-independent profile as per Fig. 4 for simplicity, after dropping hats in (2) the transformed VP reads

$$\begin{aligned} 0 =& \delta \int_0^T \Big[\int_0^{L_x} \Big(\int_0^{H_0} \Big[\frac{1}{2}\frac{L_w^2}{V} h(\phi_x - \frac{z}{h} h_x \phi_z)^2 + \frac{1}{2} V \frac{H_0^2}{h} (\phi_z)^2 \Big] \mathrm{d}z \\ &+ H_0 \Big[-\tilde{\phi}\Big(X\tilde{R}_t h_x + V h_\tau \Big) \\ &+ ghV\Big(\frac{1}{2}h - H_0 \Big) \Big]\Big|_{z=H_0} \Big)\,\mathrm{d}x \\ &+ \int_0^{H_0} \Big(L_w h \tilde{R}_t \phi \Big)\Big|_{x=0} \mathrm{d}z \Big]\,\mathrm{d}t \end{aligned} \tag{3}$$

with partial derivatives denoted by subscripts, and shorthand notation $X \equiv x - L_w, V \equiv L_w - \tilde{R}$, $\tilde{R} \equiv R(t)\Theta(L_w - x)$ and $R_t = \dot{R} = \mathrm{d}R/\mathrm{d}t$. Here $\Theta(L_w - x)$ is the Heaviside function, defined as unity for $x < L_W$ and zero elsewhere. Variations of (3) yield the transformed equations of motion, which expressions and derivations from the VP are found in [6] and in [7] based on direct transformations of the original equations of motion.

When the free surface is assumed single-valued with $z = h(x,t)$, and for a waveflap wavemaker at $x = W(z,t)$, an explicit transformation becomes more complicated, see [9]. In a vertical cross-section, this explicit transformation is as follows

$$\begin{aligned} x(\xi,\zeta,\tau) =& \frac{\xi\big(L_w - W(\zeta\frac{h(\xi,\tau)}{H_0},\tau)\big) + W(\zeta\frac{h(\xi,\tau)}{H_0},\tau)L_w}{L_w}, \\ z(\xi,\zeta,\tau) =& \frac{\zeta h(\xi,\tau)}{H_0}, \end{aligned} \tag{4}$$

in which computational-domain coordinates $\hat{x} = \xi, \hat{z} = \zeta, \tau = t$ (see Fig. 3) are used here and below, to highlight algebraic complexities. The transformation of the VP (1) with (4) is algebraically cumbersome and complex. Bridges and Donaldson [10] consider general coordinate transformations of Luke's VP in a vertical cross-section with fixed sidewalls and discuss various (including transfinite) transformations and the use of elliptical equations to model the coordinate transformations as deformations. Extending [10] by using (4), which is close in nature to a transfinite transformation, yields (details are omitted) the following transformed VP, again in a y-independent cross-section:

$$z = \zeta h/H_0, \quad x_\xi = \frac{(L_w - W)}{L_w} + \frac{\zeta}{H_0} W_z \frac{(L_w - \xi)}{L_w} h_\xi, \tag{5a}$$

$$x_\zeta = \frac{(L_w - \xi)}{L_w} W_z \frac{h}{H_0}, z_\xi = \zeta h_\xi / H_0, \quad z_\zeta = h/H_0, \tag{5b}$$

$$W = W(\zeta h/H_0, \tau), \quad W_\tau = \partial_\tau W(z,\tau)|_{z=\zeta h/H_0}, \tag{5c}$$

$$W_z = \partial_z W(z,\tau)|_{z=\zeta h/H_0}, \quad |J| = x_\xi z_\zeta - x_\zeta z_\xi \tag{5d}$$

$$\begin{aligned} 0 =& \delta \int_0^T \int_0^{L_s} \Big(-(1 - W/L_w)\phi\, h_\tau + (1 - \xi/L_W) h_\xi W_\tau \phi \\ &+ x_\xi g (\frac{1}{2} z^2 - H_0 z) \Big)|_{\zeta = H_0} \,\mathrm{d}\xi \\ &+ \int_0^{H_0} \Big(z_\zeta W_\tau \phi + x_\zeta g (\frac{1}{2} z^2 - H_0 z) \Big)|_{\xi = 0} \,\mathrm{d}\zeta \\ &+ \int_0^{L_s} \int_0^{H_0} \frac{1}{2|J|} \Big((x_\zeta^2 + z_\zeta^2) |\partial_\xi \phi|^2 \\ &- 2(x_\xi x_\zeta + z_\xi z_\zeta) \partial_\xi \phi \partial_\zeta \phi \\ &+ (x_\xi^2 + z_\xi^2) |\partial_\zeta \phi|^2 \Big) \,\mathrm{d}\xi \,\mathrm{d}\zeta \,\mathrm{d}\tau. \end{aligned} \tag{5e}$$

Both the transformed VP (3) (for waves driven by a piston wavemaker) and the transformed VP (5) (for waves driven by a waveflap wavemaker) are algebraically complex. In both cases it is still possible to parameterise the free surface with one variable $h(\hat{x}, \hat{t})$ or $h(\xi, \tau)$, in contrast to the case for a general coordinate transformation, see [10]. *Firedrake* is able to generate the relevant weak formulations in an automatic manner by providing it with: (i) a (time-discrete) VP, (ii) the relevant function spaces, and (iii) the nature and order of the finite-element expansions for ϕ, h, all of which are therefore essential features enabling efficient and timely code generation. *Firedrake* thus facilitates automatic implementation of the VPs, thereby reducing human error and time-to-development. This approach, of using VPs to automate code generation, is novel and under development.

We subsequently provide shallow-water simplifications of the above VPs, including linearised dynamics, in order to test the novel procedure. We additionally compare numerical results obtained from classical weak formulations, derived from the relevant VPs, with the above-described automated procedure by implementing the VPs directly. In order to illustrate the above ideas, VPs for shallow-water dynamics are now provided as they are less algebraic and therefore more easily comprehensible than the full potential-flow equations of motion.

2.2 Shallow-water dynamics

In shallow water, the dynamics become depth-independent, with variables $h(x,y,t) = H_0 + \eta(x,y,t), \phi(x,y,t)$ as in Fig. 5.

In one spatial dimension, the variational principle for linear and nonlinear shallow-water dynamics is a simplification of (1), as follows

$$\begin{aligned} 0 =& \delta \int_0^T \mathscr{L}_{swe}[\phi, \eta] \,\mathrm{d}t = \delta \int_0^T \int_{\alpha R(t)}^L \phi \partial_t \eta - \frac{1}{2}(H_0 + \alpha\eta)|\partial_x \phi|^2 \\ &- \frac{1}{2} g \eta^2 \,\mathrm{d}x - \left((H_0 + \alpha\eta) \dot{R} \phi \right)|_{x = \alpha R(t)} \,\mathrm{d}t; \end{aligned} \tag{6}$$

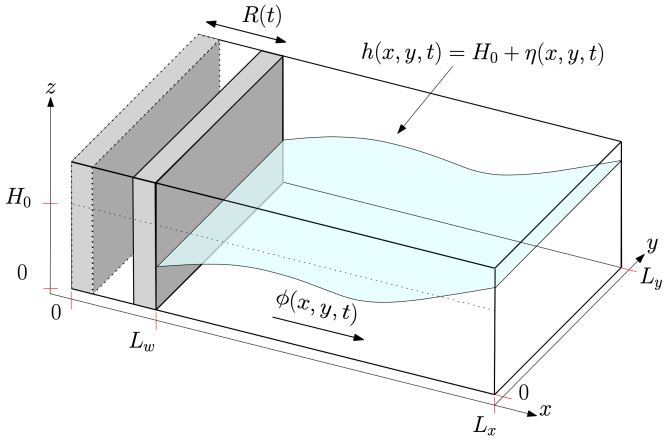

FIGURE 5: SCHEMATIC NUMERICAL WAVETANK WITH PISTON WAVEMAKER, SHOWING VARIABLES USED IN SHALLOW-WATER DYNAMICS.

when $\alpha = 0$ the dynamics resulting from varying (6) are linear and, when $\alpha = 1$, the nonlinear dynamics are recovered. Variations of (6) are defined, see e.g. [11], by

$$\delta \mathscr{L}_{swe}[\phi, \eta] \equiv \lim_{\epsilon \to 0} \frac{\mathscr{L}_{swe}[\phi + \epsilon\delta\phi, \eta + \epsilon\delta\eta] - \mathscr{L}_{swe}[\phi, \eta]}{\epsilon}$$

with the following functions as variations $\delta\eta = \delta\eta(x,t), \delta\phi = \delta\phi(x,t)$ After taking such variations of (6) with respect to ϕ and η, the following equations of motion emerge

$$h_t = \eta_t = -\partial_x \left((H_0 + \alpha\eta)\phi_x \right), \tag{7a}$$

$$\partial_t \phi = -\frac{1}{2}\alpha |\partial_x \phi|^2 - g\eta \tag{7b}$$

$$\partial_x \phi = R_t \quad \text{at} \quad x = 0, \quad \text{and} \tag{7c}$$

$$\partial_x \phi = 0 \quad \text{at} \quad x = L. \tag{7d}$$

These equations respectively comprise the continuity equation, the Bernoulli equation and the boundary conditions. The VP has a time-dependent horizontal domain $R(t) \le x \le L$ because the wavemaker position $R(t)$ is a function of time. Both the time-dependent position of the free surface $h(x,t) = H_0 + \eta(x,t)$ and the velocity potential $\phi(x,t)$ are unknown. In order to render static the mesh in the numerical discretisation, the VP (6) is transformed into a new, fixed-coordinate system in which, e.g., the new longitudinal coordinate satisfies $\xi \in [0, L]$.

The forward and backward coordinate transformations are

$$\begin{aligned} x(\xi,\tau) =& \begin{cases} R(\tau) + \dfrac{\xi(L_w - R(\tau))}{L_w} & \xi \in [0, L_w] \\ \xi & \xi \in [L_w, L] \end{cases} \\ =& \frac{\xi L_w + (L_w - \xi) R(\tau) \Theta(L_w - \xi)}{L_w}, \quad \tau = t, \end{aligned} \tag{8}$$

$$\begin{aligned} \xi(x,t) =& L_w \frac{(x - R(t))}{L_w - R(t)} \\ &- \frac{R(t)(x - L_w)\Theta(x - L_w)}{L_w - R(t)}, \quad t = \tau. \end{aligned} \tag{9}$$

Emulating the shorthand notation used immediately after (3), we define $X \equiv \xi - L_w, V(\tau) \equiv L_w - \alpha R(\tau)\Theta(L_w - \xi), \tilde{R} \equiv R(\tau)\Theta(L_w - \xi)$ and $\tilde{R}_\tau \equiv R_\tau \Theta(L_w - \xi)$. Omitting details of an otherwise straightforward derivation, the VP in the new coordinate system $\{\xi, \tau\}$ reads

$$0 = \delta \int_0^T \int_0^L \Big[\frac{1}{2}\frac{L_w^2}{V}(H_0 + \alpha\eta)(\phi_\xi)^2 - \phi(V\eta_\tau + \alpha X \tilde{R}_\tau \eta_\xi) + V\frac{1}{2} g\eta^2 \Big] \mathrm{d}\xi + L_w R_\tau \phi(H_0 + \alpha\eta)|_{\xi=0}\, \mathrm{d}\tau. \tag{10}$$

The expression (10) is similar to the transformed VP stated in equation (8) in [8] after excluding dependencies on the y and z coordinates and taking the velocity potential as a function of x and t only. As a consistency check, for linearised dynamics with $\alpha = 0$, the VP (10) is of course the same as the VP (6) with $x = \xi, t = \tau, V = L_w$ and $\alpha = 0$.

After taking variations of (10) with respect to $\delta\phi$ and $\delta\eta$, and evaluating the boundary terms by performing integration by parts, the resulting weak formulation is

$$0 = \int_0^T \int_0^L \Big(\Big[X\alpha\tilde{R}_\tau\eta_\xi + V\eta_\tau - \frac{L_w^2}{V}\partial_\xi\left((H_0 + \alpha\eta)\phi_\xi\right) \Big]\delta\phi - \Big[X\tilde{R}_\tau\phi_\xi + V\phi_\tau + \frac{1}{2}\alpha\frac{L_w^2}{V}(\phi_\xi)^2 + Vg\eta \Big]\delta\eta \Big)\, \mathrm{d}\xi + \Big(\frac{L_w^2}{V}((H_0 + \alpha\eta)\phi_\xi) - L_w R_\tau (H_0 + \alpha\eta) \Big)\Big|_{\xi=0} \delta\phi|_{\xi=0} \mathrm{d}\tau. \tag{11}$$

Since each variation $\delta\phi$ in the interior, $\delta\eta$ in the interior and $\delta\phi$ at the (transformed) piston-wavemaker location $\xi = 0$ is arbitrary, each bracketed expression prior to each variation holds pointwise in space and time. Through this observation the transformed continuity, Bernoulli and wavemaker equations emerge. Note that, in the above variations, end-point contributions arising through integration by parts in time are annihilated because of the temporal-end-point conditions $\delta\eta(\xi, 0) = \delta\eta(\xi, T) = 0$, the former of which logically follows from the specified initial condition $\eta(\xi, 0)$, whose variation is definitively zero; the latter follows by invoking symmetry in time.

Finally, we observe that the presence of wavemakers implies that the integrands in the VPs are functions of variables whose spatio-temporal dependence is both implicit and explicit, the latter reflecting that the resulting dynamics are non-autonomous. In the absence of wavemakers, the total energy $\mathcal{H}$, comprising the integral sum of kinetic and potential energy, is a conserved quantity such that $\mathrm{d}\mathcal{H}/\mathrm{d}t = 0$, and that $\mathcal{H}(t) = \mathcal{H}(t = 0)$ is independent of time. In contrast, when wavemakers are present, $\mathrm{d}\mathcal{H}/\mathrm{d}t \neq 0$ even though the total mass or water volume is conserved in a closed domain.

3. NUMERICAL MODELLING

Given the considered hierarchy of VPs for potential-flow and shallow-water continuum dynamics, the next step is their numerical implementation in both space and time within the finite-element-based environment *Firedrake* [12, 13].

The strategy will be to state and implement the VPs as directly as possible in *Firedrake*, since the VPs are already (closely) related to the required finite-element weak formulations. While the automated use of temporal discretisations of PDEs is in progress in *Firedrake*, the automated use of geometric and variational integrators in space and time therein requires more development. We therefore implement and consider time-discrete VPs next. The conservative nature of the dynamics requires that special time integrators are applied. Since the spatially-discrete dynamics remains conservative given its generation from a spatially-discrete VP without any numerical damping added, that requirement to use special integrators for stiff problems remains valid. We will therefore use so-called geometric time integrators [4, 14, 15] such as the first-order symplectic-Euler (SE) and second-order Störmer-Verlet (SV) time-integration schemes. These are explicit for linear wave dynamics but semi-implicit with a timestep restriction for nonlinear wave dynamics. Alternatively, a fully implicit second-order geometric mid-point scheme has been under consideration. The latter equates to the Crank-Nicolson time-stepping scheme for linear wave dynamics.

We now describe the spatial discretisation, briefly as it is highly automated intrinsically within *Firedrake*, followed by a description of the temporal discretisation of the VPs. The latter will be done in reverse order of complexity: first, in the VPs for (linear) shallow-water dynamics; then, in the more complicated VPs for potential-flow water-wave dynamics.

3.1 Spatial discretization

Function spaces, finite-element expansions and element types are specified directly into *Firedrake*. For testing our approach using VPs, we have used Gauss-Lobatto-Legendre (GLL) Lagrange continuous-Galerkin (CG) polynomials on linear and quadrilateral elements. Linear CG1 and higher-order CG2/CG3 polynomials have been used, leading formally to second- to fourth-order accuracy in space. Extension to three-dimensional brick elements and higher-order CGk polynomials leading to formal $(k+1)^{\text{st}}$-order accuracy in space is readily accommodated in *Firedrake*. In addition, parallel computing is built into *Firedrake* via MPI. Note that CG1 to CG4 discretisations have been employed to calculate highly nonlinear three-soliton interactions in the bidirectional Benney-Luke wave equations [16], which form a dispersive higher-order approximation to potential-flow water-wave dynamics.

3.2 Time-discrete VPs – temporal discretization

3.2.1 Shallow-water equations with piston wavemaker.

For linear shallow-water dynamics, two formulations are derived to facilitate a comparison between a numerical implementation with classical weak formulations and one using the time-discrete VPs provided below. The time-discrete weak formulations are derived by multiplying the time-discrete equations of motion found in (7), for $\alpha = 0$, by respective test functions, i.e., by $\delta\phi^n$ and $\delta\eta^{n+1}$, and integration (by parts) in space. A combined forward-Euler timestep for updating η and backward-Euler timestep for updating ϕ, forming a so called linear SE scheme, is employed.

The resulting time-discrete weak formulations are as follows

$$\int_0^L \delta\phi^n \frac{(\eta^{n+1}-\eta^n)}{\Delta t} - H_0 \boldsymbol{\nabla}\phi^n \cdot \boldsymbol{\nabla}\delta\phi^n \,\mathrm{d}x - H_0 R_t^n \delta\phi^n|_{x=0} = 0, \tag{12a}$$

$$\int_0^L \left(\frac{(\phi^{n+1}-\phi^n)}{\Delta t} + g\eta^{n+1}\right)\delta\eta^{n+1}\,\mathrm{d}x = 0. \tag{12b}$$

The corresponding combined linear and nonlinear time-discrete weak formulations are

$$\int_0^L V^n \frac{\eta^{n+1}-\eta^n}{\Delta t}\delta\phi^n - \frac{L_w^2}{V^n}(H_0+\alpha\eta^{n+1})\phi_\xi^n\,\partial_\xi(\delta\phi^n)\,\mathrm{d}\xi = \int_0^L -\alpha X\tilde{R}_\tau^n\eta_\xi^{n+1}\delta\phi^n + L_w R_\tau^n(H_0+\alpha\eta^{n+1})\delta\phi^n\Big|_{\xi=0}, \tag{13a}$$

$$\int_0^L \left(\frac{V^{n+1}\phi^{n+1}-V^n\phi^n}{\Delta t} + gV^n\eta^{n+1}\right)\delta\eta^{n+1}\,\mathrm{d}\xi = \int_0^L \alpha X\tilde{R}_\tau^n\phi^n\partial_\xi(\delta\eta^{n+1}) - \frac{1}{2}\alpha\frac{L_w^2}{V^n}(\phi_\xi^n)^2\delta\eta^{n+1}\,\mathrm{d}\xi - \alpha L_w R_\tau^n\phi^n\delta\eta^{n+1}\Big|_{\xi=0}, \tag{13b}$$

which are seen to coincide with (12), for $\alpha = 0$, when also $V = L_w$. Note that, in the nonlinear case, the conjugate variable to η is the combination $V\phi$. The geometric factor V can be evaluated at (indexed) times $n, n+1/2$ or $n+1$ for this first-order scheme; here we evaluated at n, see [4, 15]. The corresponding time-discrete analogue of the continuum VP (10) for linear/nonlinear shallow-water equations reads:

$$0 = \delta\int_0^L \Big[\phi^n\Big(\alpha X\tilde{R}_\tau\partial_\xi\eta^{n+1} + V^n\frac{\eta^{n+1}-\eta^n}{\Delta t}\Big) - V^{n+1}\phi^{n+1}\frac{\eta^{n+1}}{\Delta t} - \frac{1}{2}\frac{L_w^2}{V^n}(H_0+\alpha\eta^{n+1})|\phi_\xi^n|^2 - \frac{1}{2}gV^n\eta^{n+1})^2\Big]\,\mathrm{d}\xi - L_w R^n{}_\tau(H_0+\alpha\eta^{n+1})\phi^n|_{\xi=0}, \tag{14}$$

which is directly implemented into *Firedrake*. The above time-discrete VP is a simplified version of a systematic derivation, following work by [15, 17]. Employing the *Firedrake* (partial) "functional" derivative command `derivative` with respect to $\delta\phi^n, \delta\eta^{n+1}$ automatically generates the weak formulations to be solved numerically (see §17.5.1 in [18] and §6.4 in [19]). While the above variational approach is straightforward for shallow-water dynamics, for the (transformed) potential-flow dynamics of coupled nonlinear water-wave dynamics and dynamics of hyperelastic structures, described by coupled VPs, this automated procedure using time-discrete VPs is more effective than manual derivation.

Based on a similar systematic derivation, a time-discrete VP leading to a second-order SV time discretisation reads:

$$\begin{aligned}0 = \delta\int_0^L \Big[&-2\eta^n\Big(\frac{V^{n+1/2}\phi^{n+1/2}-V^n\phi^n}{\Delta t}\Big)\\ &- 2\eta^{n+1}\Big(\frac{V^{n+1}\phi^{n+1}-V^{n+1/2}\phi^{n+1/2}}{\Delta t}\Big)\\ &+ \alpha X\tilde{R}_\tau^{n+1/2}\Big(\partial_\xi\eta^{n+1}+\partial_\xi\eta^n\Big)\phi^{n+1/2}\\ &- \frac{1}{2}\frac{L_w^2}{V^{n+1/2}}(\phi_\xi^{n+1/2})^2\Big((H_0+\alpha\eta^{n+1})+(H_0+\alpha\eta^n)\Big)\\ &- \frac{1}{2}gV^{n+1/2}\Big((\eta^{n+1})^2+(\eta^n)^2\Big)\Big]\,\mathrm{d}\xi\\ &- L_w R_\tau^{n+1/2}\phi^{n+1/2}\Big((H_0+\alpha\eta^{n+1})+(H_0+\alpha\eta^n)\Big)\Big|_{\xi=0}.\end{aligned} \tag{15}$$

As illustration, for the case $\alpha = 0$ and $V = L_w$, variations of (15) with respect to $\delta\eta^n$, $\delta\phi^{n+1/2}$ and $\delta\eta^{n+1}$ yield the time-discrete weak formulations of linear shallow-water dynamics based on a second-order Störmer-Verlet time-stepping scheme, as follows

$$\int_0^L -2\Big(\frac{\phi^{n+1/2}-\phi^n}{\Delta t}\Big)\delta\eta^n - g\eta^n\delta\eta^n\,\mathrm{d}x = 0, \tag{16a}$$

$$\int_0^L 2\Big(\frac{\eta^{n+1}-\eta^n}{\Delta t}\Big)\delta\phi^{n+1/2} - 2H_0\partial_\xi\phi^{n+1/2}\partial_\xi(\delta\phi^{n+1/2})\,\mathrm{d}x - 2H_0R_t^{n+1/2}\delta\phi^{n+1/2}|_{x=0} = 0, \tag{16b}$$

$$\int_0^L -2\Big(\frac{\phi^{n+1}-\phi^{n+1/2}}{\Delta t}\Big)\delta\eta^{n+1} - g\eta^{n+1}\delta\eta^{n+1}\,\mathrm{d}x = 0. \tag{16c}$$

In *Firedrake*, however, we do not implement these weak formulations explicitly but instead generate the weak forms automatically from the time-discrete VP.

3.2.2 Potential-flow equations with piston wavemaker.

Presently, elliptic equations in *Firedrake* must be solved with a Dirichlet boundary condition that does not include an unknown. For consistent geometric time integrators such as SE or SV schemes, potential-flow equations require solution of Laplace's equation with the unknown $\phi(x, z = H_0, t)$ specified at the transformed free surface. Hence, we introduce a splitting of the velocity potential into a sum of its surface-bound and interior parts, i.e. $\phi(x,z,t) = \psi(x,t)\hat{\phi}(z) + \varphi(x,z,t)$ for $\hat{\phi}(H_0) = 1$, with the former $\psi(x,t) = \phi(x,H_0,t)$ and the latter zero at the free surface (in transformed coordinates), $\varphi(x,H_0,t) = 0$. To date we have mainly considered a vertical structure function $\hat{\phi}(z) = 1$ but other choices may be more optimal. Also note that $\partial_z\psi = 0$ and that the combined Neumann condition $\hat{\mathbf{n}}\cdot(\partial_x(\psi+\varphi), \partial_z\varphi) = 0$ holds at solid-wall boundaries with outward normal $\hat{\mathbf{n}}$. Consequently, this condition remains imposed naturally in the weak formulations ensuing from the time-discrete VP. The domain considered here has a flat bottom and a vertical sidewall on the right.

A first-order time-discrete analogue of the VP (3) for potential-flow dynamics with a piston wavemaker, yielding an SE time discretisation for the two conjugate kinematic and Bernoulli

equations at the free surface, then reads

$$
\begin{aligned}
0 =&\delta \int_0^{L_x}\int_0^{H_0} -\Big[\frac{1}{2}\frac{L_w^2}{V^{n+1}}h^n(\psi_x^{n+1}+\varphi_x^{n+1}+(z/h^n)h_x^n)\varphi_z^{n+1})^2 \\
&+\frac{1}{2}V^{n+1}\frac{H_0^2}{h^n}(\varphi_z^{n+1})^2\Big]\,\mathrm{d}z\,\mathrm{d}x \\
&+\int_0^{L_x} -gH_0V^{n+1}h^n(\frac{1}{2}h^n-H_0) \\
&+H_0V^{n+1}\psi^{n+1}\frac{(h^{n+1}-h^n)}{\Delta t}+H_0V^n\psi^n\frac{h^n}{\Delta t} \\
&-H_0\psi^{n+1}(x-L_w)R_t^{n+1}h_x^n\,\mathrm{d}x \\
&-\int_0^{H_0} L_wR_t^{n+1}(\psi^{n+1}+\varphi^{n+1})h^n|_{x=0}\,\mathrm{d}z\,\mathrm{d}t, \qquad (17)
\end{aligned}
$$

wherein we again notice that $V\psi$ is considered as conjugate variable to the "position" variable h. Hence, we consistently evaluate terms with explicit time dependence at discrete time level $n+1$, except for one term that links to the past. Two intrinsically coupled weak formulations follow from variations of the VP (17) with respect to $\{\delta h^n, \delta\varphi^{n+1}\}$ yielding the combined solution updates $\{\psi^{n+1}, \varphi^{n+1}\}$. The algebraic equation for ψ^{n+1} is nonlinear and coupled to a linear equation for φ^{n+1}. Herein, the Dirichlet boundary condition $\varphi^{n+1}(x, H_0, t) = 0$ is explicitly imposed at the (transformed) free surface at $z = H_0$. The final weak formulation follows from the variation of VP (17) with respect to $\delta\psi^{n+1}$, yielding an explicit update h^{n+1}.

We have similarly derived a second-order SV time-discrete VP for potential-flow equations with a piston wavemaker that reads

$$
\begin{aligned}
0 =&\delta \int_0^{L_x}\int_0^{H_0} -\Big[\frac{1}{4}\frac{L_w^2}{V^{n+1/2}}h^n\Big(\psi_x^{n+1/2}+\varphi_x^{n+1/2} \\
&+(z/h^n)h_x^n)\varphi_z^{n+1/2}\Big)^2+\Big(\frac{1}{4}\frac{L_w^2}{V^{n+1/2}}h^{n+1}(\psi_x^{n+1/2}+\varphi_x^{n+1/2} \\
&+(z/h^{n+1})h_x^{n+1})\varphi_z^{n+1/2}\Big)^2+\frac{1}{4}V^{n+1/2}\frac{H_0^2}{h^n}(\varphi_z^{n+1/2})^2 \\
&+\frac{1}{4}V^{n+1/2}\frac{H_0^2}{h^{n+1}}(\varphi_z^{n+1/2})^2\Big]\,\mathrm{d}z\,\mathrm{d}x \\
&+\int_0^{L_x} -\frac{1}{2}gH_0V^{n+1/2}h^{n+1}(\frac{1}{2}h^{n+1}-H_0) \\
&-\frac{1}{2}gH_0V^{n+1/2}h^n(\frac{1}{2}h^n-H_0) \\
&+H_0(V^{n+1/2}\psi^{n+1/2}\frac{(h^{n+1}-h^n)}{\Delta t}-V^{n+1}\psi^{n+1}\frac{h^{n+1}}{\Delta t}+V^n\psi^n\frac{h^n}{\Delta t}) \\
&-\frac{1}{2}H_0\psi^{n+1/2}(x-L_w)R_t^{n+1/2}(h_x^n+h_x^{n+1})\,\mathrm{d}x \\
&-\frac{1}{2L_w}\int_0^{H_0} R_t^{n+1/2}(\psi^{n+1/2}+\varphi^{n+1/2})(h^n+h^{n+1})|_{x=0}\,\mathrm{d}z\,\mathrm{d}t. \qquad (18)
\end{aligned}
$$

The combined variations of VP (18) with respect to $\{h^n, \varphi^{n+1/2}\}$ yield equations for the pairing $\{\psi^{n+1/2}, \varphi^{n+1/2}\}$, the latter which are solved in unison. These coupled equations are nonlinear in $\psi^{n+1/2}$ and linear in $\varphi^{n+1/2}$. Finally, the variation of VP (18) with respect to h^{n+1} yields an equation for the update ψ^{n+1}. The conjugate variable $V\psi$ is again suitably discretised in time.

Finally, the VP matching the modified midpoint (MMP) time discretisation can be derived to be

$$
\begin{aligned}
0 =&\delta\Big[-\int_0^{L_x}\int_0^{H_0}\Big[\frac{1}{2}\frac{L_w^2}{V^{n+1/2}}h^{n+1/2}(\tilde{\phi}_x^{n+1/2}+\varphi_x^{n+1/2} \\
&+\frac{z}{h^{n+1/2}}h_x^{n+1/2}\varphi_z^{n+1/2})^2+\frac{1}{2}V^{n+1/2}\frac{H_0^2}{h^{n+1/2}}(\varphi_z^{n+1/2})^2\,\mathrm{d}z\,\mathrm{d}x \\
&-\int_0^{L_x} gh^{n+1/2}V^{n+1/2}\Big(\frac{1}{2}h^{n+1/2}-H_0\Big)-\frac{1}{2}gV^{n+1/2}H_0^2\,\mathrm{d}x \\
&-\int_0^{H_0}\Big(L_wh\tilde{R}_t^{n+1/2}(\tilde{\phi}+\varphi^{n+1/2})\Big)\Big|_{x=0}\,\mathrm{d}z \\
&+\int_0^{L_x} H_0\Big(\tilde{\phi}^{n+1/2}X\tilde{R}_t^{n+1/2}h_x^{n+1/2}+V^{n+1/2}\tilde{\phi}^{n+1/2}\frac{(h^{n+1}-h^n)}{\Delta t} \\
&-h^{n+1/2}\frac{(V^{n+1}\tilde{\phi}^{n+1/2}-V^n\tilde{\phi}^n)}{\Delta t}\Big)\,\mathrm{d}x\Big]. \qquad (19)
\end{aligned}
$$

By varying it with respect to $\{\tilde{\phi}^{n+1/2}, h^{n+1/2}, \varphi^{n+1/2}\}$ in a partial way (i.e. by keeping spatial gradients on the variational perturbations), subsequent substitution of $\tilde{\phi}^{n+1} = 2\tilde{\phi}^{n+1/2} - \tilde{\phi}^n$, $h^{n+1} = 2h^{n+1/2} - h^n$, the resulting weak formulations are solved as one coupled nonlinear system for the unknowns $\tilde{\phi}^{n+1/2}, h^{n+1/2}, \varphi^{n+1/2}$.

3.3 Timestep criterion

The SE and SV schemes are conditionally stable. A linear stability criterion can be based on analysis of the linear harmonic oscillator, with frequency ω_{max} [14], as follows

$$\Delta t = CFL(2/\omega_{max}), \qquad (20)$$

where for the "CFL"-number we take $CFL \leq 1$. For linear wave dynamics, ω_{max} is the maximum wave frequency, which can be estimated using the linear, potential-flow dispersion relation

$$\omega_{max} \approx \sqrt{gk\tanh(kH_0)} \leq \sqrt{gH_0}k \qquad (21)$$

the upper bound holding in the shallow-water limit. The maximum wavenumber $k = 2\pi/\Delta x$ depends on an estimate Δx of the minimum mesh size. For nonlinear wave dynamics, the CFL (again satisfying $CFL \leq 1$) needs to be estimated and tested. Codes are anticipated to become unreliable when waves become too steep; this can be circumvented by using parametrised wave-breaking schemes such as the one in ([20]). Wave-breaking parametrisation schemes have not been considered here.

3.4 Nonlinear algebraic solvers

The described spatio-temporal discretisation of nonlinear wave dynamics results in algebraic systems of equations having both nonlinear and linear parts. These have been solved using the nonlinear solvers built into *Firedrake*, including Newton iteration and *PetSc* [13], which solvers can be made problem-specific via suitable preconditioners. Optimisation of the numerical solvers employed is in progress.

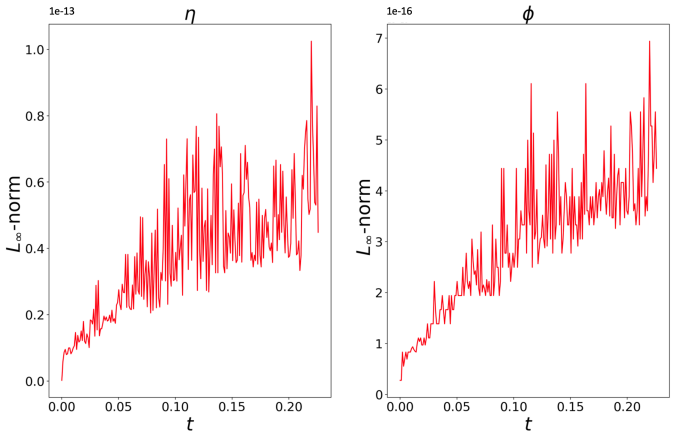

FIGURE 6: TIME EVOLUTION OF L_∞ NORMS OF THE DIFFERENCE BETWEEN NUMERICAL SIMULATIONS OF SOLUTIONS η (LEFT) AND ϕ (RIGHT), FOR THE LINEAR SHALLOW-WATER EQUATIONS, FOR CASE 1 AND CASE 2. NORMS ARE TAKEN OVER THE FULL SOLUTION DOMAIN AND EACH SUBGRAPH CONFIRMS THAT THE RESULTS OF THE TWO CASES ARE, AS EXPECTED, EQUIVALENT TO WITHIN MACHINE PRECISION. THE POSITIVE MEAN SLOPE IN BOTH PLOTS REFLECTS ERROR ACCUMULATION WITH THE EVOLVING NUMBER OF CALCULATIONS. VERTICAL AXES DISPLAY MULTIPLES OF 10^{-13} AND 10^{-16} IN LEFT- AND RIGHT-HAND PLOTS RESPECTIVELY. A CG1 SPATIAL DISCRETISATION WITH 200 ELEMENTS HAS BEEN USED.

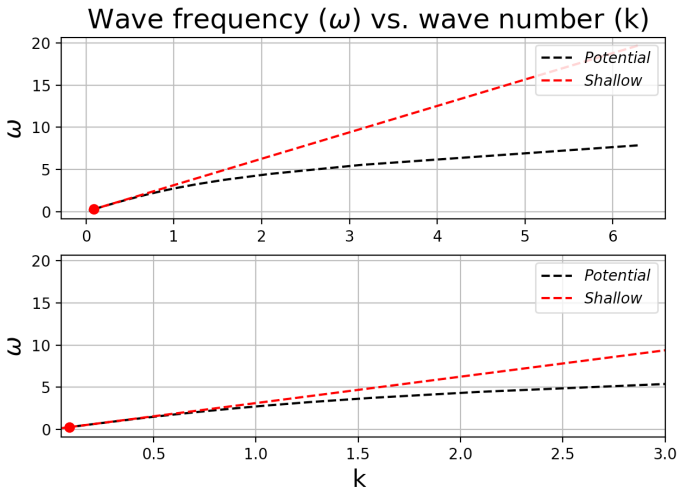

FIGURE 7: WAVE FREQUENCIES FOR POTENTIAL-FLOW (BLACK) AND SHALLOW-WATER (RED) CASES. THE RED DISC SHOWS THE CHOSEN FREQUENCY OF THE WAVEMAKER.

4. NUMERICAL TESTS

A hierarchy of increasingly complicated preliminary tests has been conducted: first, the linear shallow-water equations are implemented in two ways (see below) by way of cross-validation; second, piston-wavemaker-driven nonlinear shallow-water simulations are compared with potential-flow simulations using the code considered in [8]; and, third, preliminary simulations are conducted of nonlinear potential-flow dynamics with larger wavedriving, and based on a direct implementation of VPs (17) to (19) into *Firedrake*.

4.1 Comparison of VP and weak forms for linear shallow-water dynamics

Two approaches for solving the VP for linear shallow-water dynamics are compared. Case 1, our novel method, uses the time-discrete VP to compute time-discrete weak formulations using the derivative command in *Firedrake*. Case 2 is the traditional method that implements the time-discrete weak formulations explicitly. The numerical results for Cases 1 and 2 are, as expected, the same to machine precision, as evidenced in Fig. 6. The proposed novel approach automates the process of deriving the time-discrete weak formulations and, cross-validated via this test, it can therefore efficiently replace the traditional approach.

4.2 Comparison of driven long waves using shallow-water and potential-flow dynamics

Simulation results obtained from the presently developed numerical wavetanks based on the VPs for linear/non-linear shallow-water equations are compared with the potential-flow solver, from [8], in the small-amplitude limit for the case of waves generated from rest by a piston wavemaker. In the latter potential-flow solver, weak forms are implemented explicitly, after the vertical z-dependence in the VP is integrated out using one element in the vertical with a higher-order standard Lagrange polynomial expansion of the variables; the resulting VP then depends on only the horizontal coordinates and time. Corresponding variations yield algebraically-complex weak formulations that are subsequently implemented in *Firedrake*, cf. [6, 8].

The angular frequency of the wavemaker is chosen in such a way as to generate long waves, thereby admitting a comparison of the results obtained from shallow-water equations with those obtained by solving the potential-flow equations. The dispersion relation for wave frequency ω, as a function of wave number k, for linear potential-flow and shallow-water motion is shown, for free waves, in Fig. 7, in which the chosen wavemaker frequency is indicated by a red disc. The (static computational) domain has dimensions $L_x = 140\text{m}$ and $H_0 = 1\text{m}$; first-order piecewise-linear continuous Galerkin (CG1) polynomials are used, with 200 elements and timestep $\Delta t = 0.02\text{s}$; we furthermore employ $n_z = 4^{\text{th}}$-order Lagrange polynomials across the transformed depth. The wavemaker motion chosen and controllable parameters used are:

$$R(t) = \begin{cases} \gamma\cos(\sigma t) & 0 \le t \le T_p \\ 0 & t > T_p \end{cases}, \tag{22}$$

$$\sigma = \sqrt{gH_0}k = \sqrt{gH_0}2\pi/\lambda, \lambda = 70\text{m}, T_p = 2\pi/\sigma, \gamma = 0.002\text{m}.$$

Simulations are undertaken over two time periods $0 \le t \le 2T_p$. Initially, the wavemaker and free surface of the water are at rest. The wavemaker gradually starts from rest and stops after completing one wave period.

These simulations are seen to compare well, as evidenced by the near-coincident profiles of the free surfaces and surface-velocity potentials plotted at $t = T_p, 2T_p$ in Figs. 8 to 11. Finally, not shown here, we report that the potential-flow simulation directly implementing the VP (17) into *Firedrake* yields the same

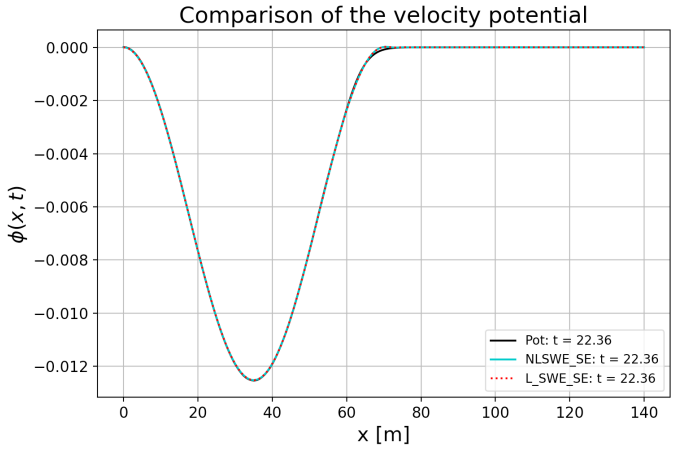

FIGURE 8: FREE-SURFACE VELOCITY POTENTIAL AFTER ONE TIME PERIOD $t = T_p$. BLACK, CYAN AND RED LINES RESPECTIVELY CORRESPOND TO POTENTIAL, NONLINEAR AND LINEAR SHALLOW-WATER SOLVERS.

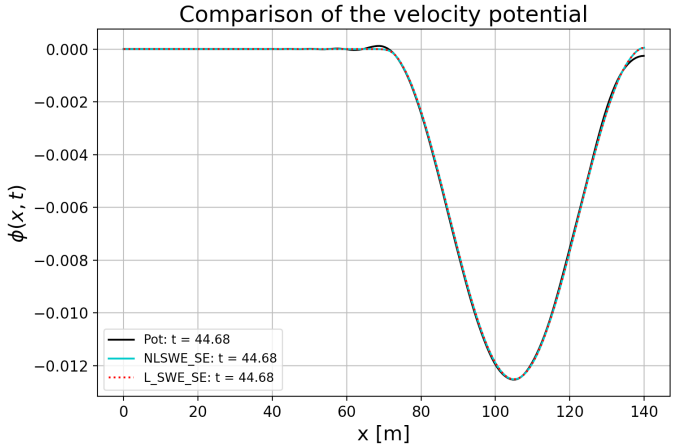

FIGURE 9: FREE-SURFACE VELOCITY POTENTIAL AT FINAL TIME $t = 2T_p$. BLACK, CYAN AND RED LINES RESPECTIVELY CORRESPOND TO POTENTIAL, NONLINEAR AND LINEAR SOLVERS.

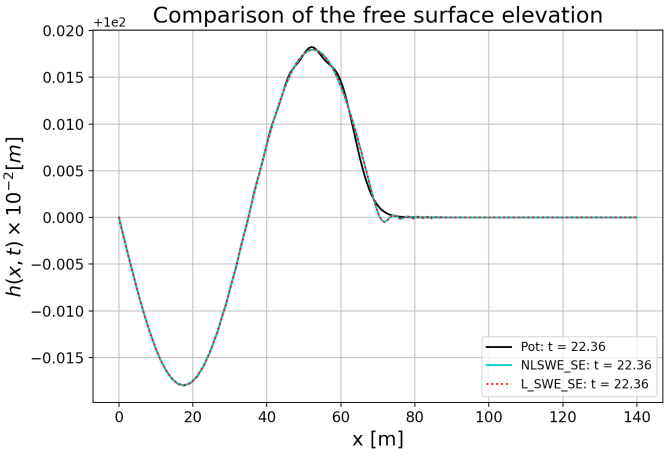

FIGURE 10: FREE-SURFACE ELEVATION AFTER ONE TIME PERIOD $t = T_p$. BLACK, CYAN AND RED LINES RESPECTIVELY CORRESPOND TO POTENTIAL, NONLINEAR AND LINEAR SOLVERS.

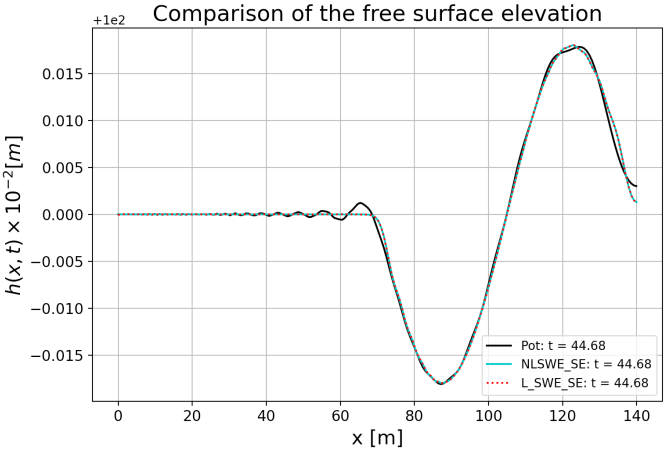

FIGURE 11: FREE-SURFACE ELEVATION AT FINAL $t = 2T_p$. BLACK, CYAN AND RED LINES RESPECTIVELY CORRESPOND TO POTENTIAL-FLOW, NONLINEAR AND LINEAR SOLVERS.

results as those obtained from this potential-flow simulation.

Preliminary simulations of the potential-flow discretisation based on the novel MMP-VP-based approach (19) as well as with SV and SE time discretisations show consistent results for piston-driven flows with larger piston amplitude $\gamma = 0.5$m. Finally, waveflap/piston-driven wave simulations for η and ϕ at the free surface are shown in Fig. 12, for the final five of 30 wave-forcing periods, using (5) in the piston-wavemaker limit. Piston motion at $x = W(z,t) = R(t) = -\gamma\cos(\sigma t)$ and $\gamma = 0.2$m and the MMP time-discrete version (19) have been implemented in *Firedrake*. Note that this implementation has also been shown to replicate the results of the earlier MMP-SV-SE potential-flow implementations in the piston-wavemaker limit for $W(z,t) = R(t)$. The corresponding kinetic, potential and total energy evolutions are shown in Fig. 13, which reveals that the wavemaker on average injects energy into the system but, when it stops after $t = 28T_p$, the energy oscillations are (as evidenced by closer inspection) bounded, with amplitude less than $10^{-3}\%$ of their base value. Verification and validation tests are under way. In all presented cases, solutions are shown in the transformed domain.

5. CONCLUSION

We have presented novel spatio-temporal discrete finite-element numerical schemes for potential-flow and shallow-water wave dynamics based on variational principles (VPs), including extended formulations of these principles in which waves are driven by either piston or waveflap wavemakers at one end of the wavetank. The finite-element methods have been implemented in the finite-element environment *Firedrake*, whose intrinsic domain-specific compiler-architecture has, through validation of automated derivations (see below), allowed us to demonstrate a reduction in time-to-implementation, thereby offering promise to extend the approach to more complex coupled water-wave dynamics with FSI. A novel feature is that we have developed and tested the numerical implementations of the dynamics via consistent (i.e. stable and conservative) geometric time-

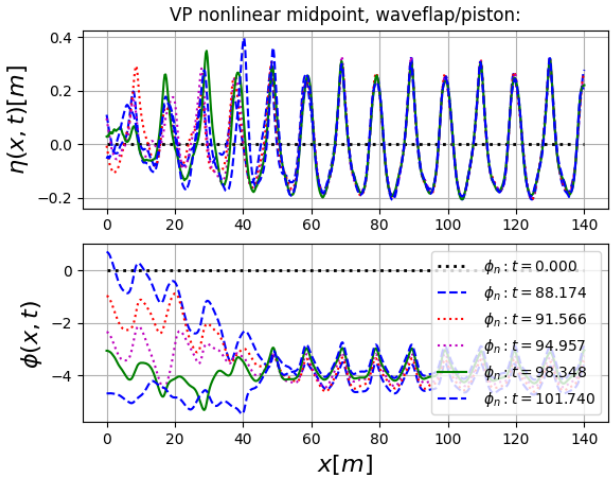

FIGURE 12: ELEVATION OF (TOP), AND VELOCITY POTENTIAL AT (BOTTOM), THE FREE SURFACE FOR PROFILES $25T_p \leq t \leq 30T_p \approx 105.1$s. PARAMETERS USED: 560 ELEMENTS IN THE HORIZONTAL AND 6 IN THE VERTICAL, FOR CG2 POLYNOMIALS; MMP; $\Delta t = 0.0068$s. THE EVOLUTION IS SEEN TOWARDS STANDING-WAVE PROFILES. USING WAVELENGTH $\lambda = 10$m AND FORCING FREQUENCY $\sigma = 2\pi/T_p$ DETERMINED BY LINEAR DISPERSION. PROFILES APPEAR JUST RESOLVED AT THIS RESOLUTION.

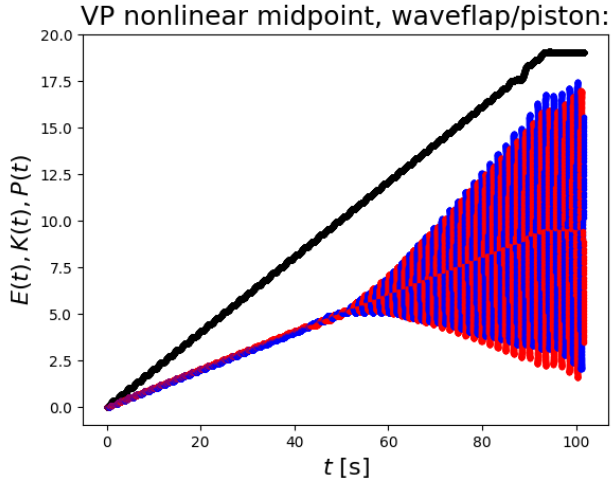

FIGURE 13: EVOLUTION OF KINETIC (RED), POTENTIAL (BLUE) AND TOTAL (BLACK) ENERGY, WHICH GROWS DUE TO THE WAVE-MAKER INPUT UNTIL $t = 28T_p$. HOWEVER, ENERGY OSCILLATIONS REMAIN SMALL AND BOUNDED ONCE THE WAVEFLAP IS SWITCHED OFF AT $t = 28T_p$.

discrete VPs, whence the discrete evolution equations are generated automatically within *Firedrake* and subsequently solved via its inbuilt (non)linear solvers. Preliminary numerical tests are therefore promising, and a full and further optimised implementation – through a time-discrete VP and verification/validation of potential-flow dynamics driven by waveflaps – is in progress.

ACKNOWLEDGMENTS

The authors acknowledge funding from the Marie Skłodowska-Curie Fellowship in the European Union European Industrial Doctorate (EID) program in the collaborative project "Eagre/Aegir: High-seas wave-impact modelling" (project number GA 859983), held by the University of Leeds and the Maritime Research Institute Netherlands (MARIN). We are grateful to Dr. Tim Bunnik (MARIN) for helpful comments. We also keenly acknowledge the crucial assistance of Colin Cotter and Koki Sagiyama from the *Firedrake* team.

REFERENCES

[1] Rehman, W., Bunnik, T., Bokhove, O. and Kelmanson, M. "Experimental Modeling of Water-Wave Interactions with a Flexible Beam." *Proc. ASME 2023 42nd Int. Conf. on Ocean, Offshore and Arctic Eng.*: p. 10. 2023. ASME.

[2] Luke, J. C. "A variational principle for a fluid with a free surface." *J. Fluid Mechanics* Vol. 27 No. 2 (1967): pp. 395–397.

[3] Brink, F.-J., Ferenc Izsák, F. and van der Vegt, J.J.W. "Hamiltonian Finite Element Discretization for Nonlinear Free Surface Water Waves." *J. Sci. Comp.* Vol. 73 (2017): pp. 366–394.

[4] Gagarina, E., Ambati, V.R., Nurijanyan, S., van der Vegt, J.J.W. and Bokhove, O. "On variational and symplectic time integrators for Hamiltonian systems." *J. Comput. Phys.* Vol. 306 (2016): pp. 370–389.

[5] Kurnia, R., M.R., Badriana and van Groesen, E. "Hamiltonian Boussinesq Simulations for Waves Entering a Harbor with Access Channel." *J. Waterway, Port, Coastal, and Ocean Eng.* Vol. 144 (2017).

[6] Gidel, F. "Variational water-wave models and pyramidal freak waves." Ph.D. Thesis, University of Leeds. 2018. https://etheses.whiterose.ac.uk/21730/.

[7] Engsig-Karup, A.P., Bingham, H.B. and Lindberg, O. "An efficient flexible-order model for 3D nonlinear water waves." *J. Comput. Phys.* Vol. 228 (2009): pp. 2100–2118.

[8] Gidel, F., Lu, Y., Bokhove, O. and Kelmanson, M.A. "Variational and numerical modelling strategies for cost-effective simulations of driven free-surface wave." (2022). URL https://eartharxiv.org/repository/view/3411/.

[9] Bokhove, O. "Variational water-wave modeling: from deep water to beaches." *The Mathematics of Marine Modelling*. Springer (2022): pp. 103–134.

[10] Bridges, T. J. and Donaldson, N. M. "Variational principles for water waves from the viewpoint of a time-dependent moving mesh." *Mathematika* Vol. 57 No. 1 (2011): pp. 147–173.

[11] Lanczos, C. *The variational principles of mechanics*. Courier Corporation (2012).

[12] Rathgeber, F., Ham, D. A., Mitchell, L., Lange, M., Luporini, F., McRae, A.W.T.T, Bercea, G.T., Markall, G.R. and Kelly, P.H.J. "Firedrake: automating the finite element method by composing abstractions." *ACM Transactions on Mathematical Software (TOMS)* Vol. 43 No. 3 (2016): pp. 1–27.

[13] Balay, S., Abhyankar, S., Adams, M., Brown, J., Brune, P., Buschelman, K., Dalcin, L., Eijkhout, V., Gropp, W., Kaushik, D. et al. "Petsc users manual revision 3.8." Technical report no. Office of Scientific and Technical Information (OSTI). 2017.

[14] Hairer, E., Hochbruck, M., Iserles, A. and Lubich, C. "Geometric numerical integration." *Oberwolfach Reports* Vol. 3 No. 1 (2006): pp. 805–882.

[15] Bokhove, O. and Kalogirou, A. "Variational water wave modelling: from continuum to experiment." *Bridges, T., Groves, M., and Nicholls, D., LMS Lecture Note Series, Cambridge University Press* Vol. 426 (2016): pp. 226–260.

[16] Choi, J., Bokhove, O., Kalogirou, A. and Kelmanson, M. A. "Numerical experiments on extreme waves through oblique-soliton interactions." *Water Waves* Vol. 4 (2022): pp. 139–179.

[17] Gagarina, E. "Variational approaches to water wave simulations." Ph.D. Thesis, University of Twente. 2014.

[18] Alnaes, M.S. *UFL: a finite element form language*. In: Automated Solution of Differential Equations by the Finite Element Method by Logg, and Mardal and Wells (Eds) (2011).

[19] Alnaes, M.S., Logg, A., Oelgaard, K.B., Rognes, M.E. and G.N., Wells. "Unified Form Language: A domain-specific language for weak formulations of partial differential equations." Technical report no. 2013. URL https://arxiv.org/pdf/1211.4047.pdf.

[20] Wang, W., Pakozdi, C., Kamath, A. and Bihs, H. "A fully nonlinear potential flow wave modelling procedure for simulations of offshore sea states with various wave breaking scenarios." *Applied Ocean Res.* Vol. 117 (2021): p. 102898.

[21] Choi, J., Kalogirou, A., Lu, Y., Bokhove, O. and Kelmanson, M. "A study of extreme water waves using a hierarchy of models based on potential-flow theory." *Water Waves* Vol. 4 (2024): pp. 139–179.

APPENDIX A. STÖRMER-VERLET TIME SCHEME –SV

Consider the VP for a one-degree-of-freedom Hamiltonian system in time[2]

$$0 = \delta \int_0^T p\frac{\mathrm{d}q}{\mathrm{d}t} - H(q,p)\,\mathrm{d}t \tag{23}$$

with Hamiltonian (energy) $H(q,p)$. We start from an Ansatz based on the work on discontinuous Galerkin finite-element time-stepping scheme in Gagarina's thesis [17]. The Ansatz for the time-discrete VP is

$$\begin{aligned} 0 =& \delta\Big(p^{n+1/2}(q^{n+1}-q^n) - q^{n+1}p^{n+1} + p^n q^n \\ & - \frac{1}{2}\Delta t\big(H(q^n,p^{n+1/2}) + H(q^{n+1},p^{n+1/2})\big)\Big), \end{aligned} \tag{24}$$

considering variations $\{q^n, p^{n+1/2}, q^{n+1}\}$. These variations then yield

$$\delta q^n: \quad p^{n+1/2} = p^n - \frac{1}{2}\Delta t\frac{\partial H(q^n,p^{n+1/2})}{\partial q^n} \tag{25a}$$

$$\delta p^{n+1/2}: \quad q^{n+1} = q^n + \frac{1}{2}\Delta\Big(\frac{\partial H(q^n,p^{n+1/2})}{\partial p^{n+1/2}} + \frac{\partial H(q^{n+1},p^{n+1/2})}{\partial p^{n+1/2}}\Big) \tag{25b}$$

$$\delta q^{n+1}: \quad p^{n+1} = p^{n+1/2} - \frac{1}{2}\Delta t\frac{\partial H(q^{n+1},p^{n+1/2})}{\partial q^{n+1}}, \tag{25c}$$

in which the first two steps are in principle implicit and the last step is (semi-)explicit.

The SV time-discrete version of VP (32a) in [15] of the Benney-Luke equations is

$$\begin{aligned} 0 =& \delta\iint_{\Omega_h} \eta^{n+1/2}\frac{(\Phi^{n+1}-\Phi^n)}{\Delta t} - \eta^{n+1}\frac{\Phi^{n+1}}{\Delta t} + \eta^n\frac{\Phi^n}{\Delta t} \\ & + \frac{\mu}{2}\nabla\eta^{n+1/2}\cdot\frac{(\nabla\Phi^{n+1}-\nabla\Phi^n)}{\Delta t} \\ & - \frac{\mu}{2}\nabla\eta^{n+1}\cdot\frac{\nabla\Phi^{n+1}}{\Delta t} + \frac{\mu}{2}\nabla\eta^n\cdot\frac{\nabla\Phi^n}{\Delta t} \\ & + \frac{1}{4}(1+\epsilon\eta^{n+1/2})(|\nabla\Phi^n|^2 + |\nabla\Phi^{n+1}|^2) + \frac{1}{2}(\eta^{n+1/2})^2 \\ & \quad + \frac{1}{2}\mu\Big(\nabla q^n\cdot\nabla\Phi^n - \frac{3}{4}(q^n)^2\Big) \\ & \quad + \frac{1}{2}\mu\Big(\nabla q^{n+1}\cdot\nabla\Phi^{n+1} - \frac{3}{4}(q^{n+1})^2\Big)\,\mathrm{d}x\,\mathrm{d}y, \end{aligned} \tag{26}$$

wherein variations are taken with respect to $\{\Phi^n, q^n; \eta^{n+1/2}; \Phi^{n+1}, q^{n+1}\}$ in turn. Assuming that we know q^n, except for $n=0$, the variation and solve for q^n is superfluous.

Application of the above (25) to the potential-flow equations yields the time-discrete SV-VP (18).

APPENDIX B. MODIFIED MIDPOINT TIME SCHEME –MMP

The goal is to find a suitable time-discrete VP yielding the modified midpoint scheme[3]. Consider the VP for a one-degree-of-freedom Hamiltonian system in time

$$0 = \delta\int_0^T p\frac{\mathrm{d}q}{\mathrm{d}t} - H(q,p)\,\mathrm{d}t \tag{27}$$

with Hamiltonian (energy) $H(q,p)$. We start from an Ansatz based on the work on discontinuous Galerkin finite-element time-stepping scheme in Gagarina's thesis [17]. The Ansatz for the time-discrete VP is

$$\begin{aligned} 0 =& \delta\Big(p^{n+1/2}(q^{n+1}-q^n) - q^{n+1/2}(p^{n+1}-p^n) \\ & + \frac{1}{2}(p^{n+1}-p^n)(q^{n+1}+q^n) + \frac{1}{2}q^n(p^n-p^{n-1}) \\ & + q^n p^{n-1/2} - q^{n-1/2}p^n + \frac{1}{2}p^n q^{n-1} \\ & \quad - \Delta t H(q^{n+1/2},p^{n+1/2})\Big), \end{aligned} \tag{28}$$

[2] Additional appendices are provided which have been derived by, used by and are copyright of OB, so not of ASME. These derivations have also been used in [21].

[3] Extra notes to OMAE article.

considering variations of this VP with respect to $\{q^{n+1/2}, p^{n+1/2}, q^n, p^n\}$. These variations of (28) are

$$\delta p^{n+1/2}: \quad q^{n+1} - q^n - \Delta t \frac{\partial H(q^{n+1/2}, p^{n+1/2})}{\partial p^{n+1/2}} = 0 \tag{29a}$$

$$\delta p^{n+1/2}: \quad p^{n+1} - p^n + \Delta t \frac{\partial H(q^{n+1/2}, p^{n+1/2})}{\partial q^{n+1/2}} = 0 \tag{29b}$$

$$\delta q^n: \quad -p^{n+1/2} + \frac{1}{2}(p^{n+1} - p^n) + p^{n-1/2} + \frac{1}{2}(p^n - p^{n-1}) = 0 \tag{29c}$$

$$\delta p^n: \quad q^{n+1/2} - \frac{1}{2}(q^{n+1} + q^n) - q^{n-1/2} + \frac{1}{2}(q^n + q^{n-1}) = 0 \tag{29d}$$

starting with $q^{-1/2} = \frac{1}{2}(q^0 + q^{-1})$ and $p^{-1/2} = \frac{1}{2}(p^0 + p^{-1})$ for $n = 0$. It is tedious to find a closed-form VP without linking from $n = 0$. Instead, consider

$$0 = \delta\left(p^{n+1/2}(q^{n+1} - q^n) - q^{n+1/2}(p^{n+1} - p^n) - \Delta t H(q^{n+1/2}, p^{n+1/2})\right), \tag{30}$$

with respect to $\delta q^{n+1/2}, \delta p^{n+1/2}$ only and then impose $q^{n+1/2} = \frac{1}{2}(q^n + q^{n+1})$ and $p^{n+1/2} = \frac{1}{2}(p^n + p^{n+1})$ to solve for the coupled system.

By applying the above to the VP (3) for potential-flow dynamics in the transformed coordinate space, we arrive at the following time-discrete VP:

$$\begin{aligned} 0 = \delta\Big[&- \int_0^{L_x} \int_0^{H_0} \Big[\frac{1}{2}\frac{L_w^2}{V^{n+1/2}} h^{n+1/2}(\tilde{\phi}_x^{n+1/2} + \varphi_x^{n+1/2} \\ &+ \frac{z}{h^{n+1/2}} h_x^{n+1/2} \varphi_z^{n+1/2})^2 + \frac{1}{2} V^{n+1/2} \frac{H_0^2}{h^{n+1/2}} (\varphi_z^{n+1/2})^2 \,\mathrm{d}z\,\mathrm{d}x \\ &- \int_0^{L_x} g h^{n+1/2} V^{n+1/2} \Big(\frac{1}{2} h^{n+1/2} - H_0\Big) - \frac{1}{2} g V^{n+1/2} H_0^2 \,\mathrm{d}x \\ &- \int_0^{H_0} \Big(L_w h \tilde{R}_t^{n+1/2}(\tilde{\phi} + \varphi^{n+1/2})\Big)\Big|_{x=0} \mathrm{d}z \\ &+ \int_0^{L_x} H_0 \Big(\tilde{\phi}^{n+1/2} X \tilde{R}_t^{n+1/2} h_x^{n+1/2} + V^{n+1/2} \tilde{\phi}^{n+1/2} \frac{(h^{n+1} - h^n)}{\Delta t} \\ &- h^{n+1/2} \frac{(V^{n+1}\tilde{\phi}^{n+1/2} - V^n \tilde{\phi}^n)}{\Delta t}\Big) \mathrm{d}x\Big]. \end{aligned} \tag{31}$$

By varying it with respect to $\{\tilde{\phi}^{n+1/2}, h^{n+1/2}, \varphi^{n+1/2}\}$ in a partial way (i.e. by keeping spatial gradients on the variational perturbations), subsequent substitution of $\tilde{\phi}^{n+1} = 2\tilde{\phi}^{n+1/2} - \tilde{\phi}^n$, $h^{n+1} = 2h^{n+1/2} - h^n$, the resulting weak formulations are solved as one coupled nonlinear system for the unknowns $\tilde{\phi}^{n+1/2}, h^{n+1/2}, \varphi^{n+1/2}$.

The modified-midpoint time-discrete version of VP (32a) in [15] of the Benney-Luke equations is

$$\begin{aligned} 0 = \delta \iint_{\Omega_h} &\eta^{n+1/2} \frac{(\Phi^{n+1} - \Phi^n)}{\Delta t} - \Phi^{n+1/2} \frac{(\eta^{n+1} - \eta^n)}{\Delta t} \\ &+ \frac{\mu}{2} \nabla \eta^{n+1/2} \cdot \frac{(\nabla \Phi^{n+1} - \nabla \Phi^n)}{\Delta t} - \frac{\mu}{2} \nabla \Phi^{n+1/2} \cdot \frac{(\nabla \eta^{n+1} - \nabla \eta^n)}{\Delta t} \\ &+ \frac{1}{2}(1 + \epsilon \eta^{n+1/2}) |\nabla \Phi^{n+1/2}|^2 + \frac{1}{2}(\eta^{n+1/2})^2 \\ &+ \mu\Big(\nabla q^{n+1/2} \cdot \nabla \Phi^{n+1/2} - \frac{3}{4}(q^{n+1/2})^2\Big) \mathrm{d}x\,\mathrm{d}y. \end{aligned} \tag{32}$$

Initial estimates indicate that this modified-midpoint discretisation based on the above VP is 1.5× faster on a MacBook than the Störmer-Verlet discretisation using weak forms, as used in [15].